IEEE Access
Multidisciplinary ⋮ Rapid Review ⋮ Open Access Journal

Received 10 December 2023, accepted 23 December 2023, date of publication 29 December 2023,
date of current version 5 January 2024.

Digital Object Identifier 10.1109/ACCESS.2023.3348121

RESEARCH ARTICLE

Single Image Enhancement Using Gradient-Norm-Based Tone Curve for Images Captured in Wide-Dynamic-Range Scenes

SEIICHI KOJIMA, (Graduate Student Member, IEEE), AND NORIAKI SUETAKE, (Member, IEEE)
Graduate School of Science and Technology for Innovation, Yamaguchi University, Yamaguchi 753-8512, Japan

Corresponding author: Seiichi Kojima (c002wbw@yamaguchi-u.ac.jp)

This work was supported by the Japan Society for the Promotion of Science (JSPS) KAKENHI under Grant JP23KJ1657.

ABSTRACT When a wide range of luminance levels exist in a scene, an image captured in the scene contains very dark and bright areas with low visibility. Various methods for improving the visibility of such images have been proposed. However, the performance of these methods is not often satisfactory owing to over-enhancement such as noise amplification. Furthermore, some methods have high computational costs. In this paper, we propose an image enhancement method for improving the visibility of images captured in wide-dynamic-range scenes. The proposed method generates a tone curve for brightness and contrast enhancements. To suppress over-enhancement, the tone curve is generated by using the gradient-norm-based weighted histogram. Applying a tone curve in a pixel-wise manner may decrease the local contrast in some regions as any tone curve has a small slope in some areas. To prevent contrast reduction, the local contrast correction for controlling the effect of the tone curve in a region-adaptive manner is introduced as the post-processing of tone curve. By applying the tone curve and local contrast correction, the proposed method can enhance the visibility of an image sufficiently while suppressing over-enhancement. In addition, each processing of the proposed method is simple and suitable for fast implementation.

INDEX TERMS Image enhancement, gradient norm, histogram, wide-dynamic-range scenes.

I. INTRODUCTION

If one were to take a photograph of the inside of a tunnel from the outside under clear skies, the image acquired will have a mixture of very dark and bright areas with low visibility. In general, it is difficult to take high-quality images in a situation wherein a wide range of luminance levels exist.

By merging multiple images captured with various exposure settings into one image, a relatively high-quality image can be acquired [1], [2], [3], [4], [5], [6]. However, such a technique tends to cause artifacts called ''ghosts'' due to misalignment between images. In addition, applying such a technique to video processing is challenging because obtaining and merging multiple images with varying exposure settings are time-consuming. Therefore, the single image enhancement method, which generates a high-quality image using a single image as input, remains highly important. General image processing methods such as histogram equalization [7], [8] cannot sufficiently enhance the quality of images captured in wide-dynamic-range scenes. Hence, dedicated algorithms are necessary for enhancing the quality of such images. Various methods for improving the visibility of an image in which very bright and dark regions exist simultaneously have been proposed [9], [10], [11], [12], [13], [14], [15], [16], [17], [18], [19], [20], [21], [22], [23], [24], [25]. Some methods use image fusion method [18], [19], [20], [21], [22], [23], [24], while others use histogram stretching [9], [10], Retinex models [13], [14], [15], [16], [17] or deep learning models [25]. For improving the visibility of images, these methods brighten dark areas of the input

The associate editor coordinating the review of this manuscript and approving it for publication was Jiafeng Xie.

image and enhance the contrast of the image. However, these methods tend to cause over-enhancement such as noise amplification and black-out or white-out. Furthermore, while it is important to keep computational costs low, some methods are problematic in terms of memory usage and time required for processing.

In this paper, we propose a method of improving the visibility of a single input image in which very bright and dark regions exist simultaneously. First, the proposed method generates a gradient-norm-based weighted histogram. Second, a tone curve that adjusts image brightness and enhances image contrast simultaneously is generated by using the weighted histogram. The slope of the tone curve is controlled, taking into account the gradient norm, which suppresses over-enhancement in flat regions. In addition, the tone curve enhances the visibility of the image by brightening very dark regions and darkening very bright regions. On the other hand, the tone curve may decrease the local contrast in some regions as the tone curve is applied not in a region-adaptive manner but in a pixel-wise manner. Hence, after applying the tone curve, the local contrast correction is applied. The local contrast correction is performed by the alpha blending of the input image and the resultant image of the tone curve. To compute the alpha value in the alpha blending, first, a bilateral filter [26], [27], [28] is applied to the input image for calculating the local average pixel values. Then, the blending coefficient is calculated so that the region prone to the local contrast reduction caused by the tone curve becomes close to the input image in the alpha blending output. The local contrast correction can suppress the local contrast reduction in the detailed regions of the image. The proposed method is fast and effectively enhances the visibility of the images containing bright and dark regions. The effectiveness of the proposed method is verified through qualitative and quantitative evaluations. Note that the word ''Single'' is used in this paper to make it clear that we are proposing a method for acquiring a high-visibility image using a single image as input without using multi-exposure images.

The contribution of our study is summarized as follows: Our proposed method addresses the challenge of obtaining high-quality images in wide-dynamic-range scenes using a single image as input while suppressing artifacts such as over-enhancement and halo artifacts. Our proposed method includes a new tone curve generation scheme, which achieves both of brightness adjustment and contrast enhancement while suppressing over-enhancement. The proposed method also includes a new local contrast correction method for suppressing local contrast reduction often caused by a tone curve based image enhancement. Each processing of the proposed method is simple and suitable for fast implementation. Hence, our method can be easily implemented as a pre-processing step for various CI applications including segmentation, object recognition and scene analysis used in the embedded devices such as surveillance cameras and automatic drone photography. We believe that our proposed method has the potential impact on CI applications.

The rest of this paper is organized as follows. The related works are described in Sect. II. The proposed method is explained in detail in Sect. III. In Sect. IV, experimental results are shown and discussed. Finally, we conclude the paper in Sect. V.

II. RELATED WORKS

A. EXPOSURE FUSION

Exposure fusion [1], [2], [3], [4], [5], [6] is an attractive method of obtaining high-quality images in a situation wherein a wide range of luminance levels exist. In exposure fusion, multi-exposure images, which are multiple images taken under different exposure conditions (in most cases, the exposure time is varied), are fused to obtain a single output image. In most cases, there are some misalignments between differently exposed images owing to moving objects in the scene and camera motion. The misalignments cause artifacts called ''ghosts'' in the fused image. Although fusion methods that are robust against ghosting [4], [6] have been proposed, their performance is not perfect, and it is difficult to completely eliminate ghosts in a wide variety of scenes. It is also difficult to reduce the computational cost required to take multiple images of a scene and fuse them, making it difficult to apply exposure fusion to video processing.

B. SINGLE IMAGE ENHANCEMENT

Histogram Equalization (HE) [7] and Contrast Limited Adaptive Histogram Equalization (CLAHE) [8] are well-known contrast enhancement methods. Although these methods can improve image contrast, they do not adjust image brightness explicitly. Hence, visibility is often not sufficiently improved for images with very dark and bright areas. In addition, HE and CLAHE tend to cause over-enhancement. To simultaneously obtain the effect of contrast enhancement by HE and brightness adjustment by gamma correction, Huang et al. proposed the adaptive gamma correction [9]. In the adaptive gamma correction, the parameter of the gamma correction is determined based on the normalized cumulative histogram of the input image. If the entire image is dark, the adaptive gamma correction can brighten an image sufficiently. However, if there are many bright regions in the input image, such as in a backlit image, the effect of brightness adjustment is not sufficient and a dark output image is obtained. Recently, Mukaida et al. [10] proposed a low-light image enhancement method extended from HE. In their method, modified gamma correction is applied to convex combination coefficients [11], [12] of the input image. Then, contrast enhancement is applied to the output of the modified gamma correction by using gamma filtering-based histogram specification. Although Mukaida et al.'s method is effective in brightening dark regions, it tends to over-brighten bright regions, making it difficult to see them. Mukaida et al.'s method also has a problem of generating images with low contrast and low visibility throughout the image.

Retinex-based image enhancement methods [13], [14], [15], [16], [17] are suitable for images captured under non-uniform illumination conditions. In these methods, each pixel value of the input image is decomposed into reflectance and illumination. By adjusting illumination, the visibility of the input image is improved. Fu et al. formulated a cost function for edge-preserving reflectance and illumination decomposition by using the L1 norm in the logarithmic domain [15]. Fu et al.'s method requires a long computation time to solve the minimization problem of the cost function. For low-light image enhancement, Guo et al. proposed a method of extracting the illumination components [16]. In Guo et al.'s method, the reflectance is calculated by simply dividing the pixel value by the illumination, allowing for fast calculations. However, when the input image has bright areas, these bright areas are prone to white-out by illumination adjustment. In addition, Guo et al.'s method tends to cause over-enhancement in flat regions. Hao et al. proposed a Retinex model using the Gaussian total variation for a regularization term [17]. Compared to the conventional Retinex model, the optimization process of Hao et al.'s model is simple. However, the optimization process is still time-consuming and not suitable for real-time applications. In addition, Hao et al.'s method tends to flatten details in dark regions.

Various image enhancement methods have been proposed for backlit images [18], [20], [21], [22], [23], [24], [25]. Wang et al. proposed a backlit image enhancement method that generates three types of intensity-transformed image and combines them by exposure fusion [18]. The three intensity-transformed images are generated by log-transformation, gamma correction and the generalized unsharp masking (GUM) [19]. Wang et al.'s method tends to amplify small noise as GUM amplifies noise in flat regions. Buades et al. performed fusion-based image enhancement for each RGB component and merged the outputs into one image [21]. In their method, the images generated by a multi-parameter gamma correction and a log function are fused and the sharpening is then applied to the fused image. Although Buades et al.'s method sharpens the details, it does not improve the global contrast sufficiently. Hence, the poor-visibility output image is generated. Ueda et al. proposed a fusion-based backlit image enhancement method using the S-type tone curve [23]. For contrast enhancement, Ueda et al.'s method applies S-type tone curves to convex combination coefficients [11], [12] of the input backlit image with various parameter settings. The output image is obtained by fusing the generated contrast-enhanced images. Ueda et al.'s method requires the creation of a very large number of images (more than 10) to obtain a good resulting image, which requires a large amount of memory and a long computation time. In addition, contrast enhancement by the S-type tone curve can cause black-out of dark areas. For backlit image enhancement, Akai et al. generated two images with improved image quality in the dark and bright regions of the image and blended them with a simple alpha blending [24]. To improve the image quality in dark areas, the brightness is adjusted by gamma correction and the contrast is enhanced by S-shaped function. For bright regions, only brightness adjustment is applied. Akai et al.'s method tends to brighten inherently dark regions such as shadows of objects, making it difficult to see details. In general, fusion-based image enhancement methods such as Wang et al.'s method have the disadvantage that the final fusion result is not always sufficiently bright, even if brightness-adjusted images are generated.

To enhance the visibility of images captured under poor lighting conditions, Guo et al. proposed a learning-based image enhancement method called Zero-Reference Deep Curve Estimation (ZERO-DCE) [25]. Guo et al.'s method adjusts image brightness by repeatedly applying a tone curve to the input image on a deep learning network. Although Guo et al.'s method is very fast, it tends to cause over-enhancement and contrast reduction that are difficult to control. In general, learning-based image processing algorithms tend to require a large network size, which results in requiring high power consumption and memory usage. Hence, learning-based image enhancement algorithms have demerits for applications that require low power consumption and memory usage (e.g., surveillance cameras and automatic drone photography). In such applications, image enhancement is often introduced as a pre-processing, which is desired to be implemented as simple as possible.

III. PROPOSED METHOD

A. NOTATIONS

In this section, the notations used in this paper are described.

The height and width of an image are denoted as U and V, respectively. The position of each pixel is represented by a two-dimensional vector $\boldsymbol{p} = (u, v)$, where $u \in \{1, 2, \cdots, U\}$, $v \in \{1, 2, \cdots, V\}$. The pixel value of a monochrome image I at position $\boldsymbol{p}$ is denoted as $I(\boldsymbol{p})$.

The maximum intensity value is denoted as l_{MAX}. For example, $l_{\mathrm{MAX}} = 255$ for an 8-bit image. The middle intensity value is denoted as l_{MID}. l_{MID} is calculated as $l_{\mathrm{MID}} = \mathrm{round}\left(\frac{l_{\mathrm{MAX}}}{2}\right)$. Let h be the histogram for I. h is defined as follows:

$$h(l) = \sum_{\boldsymbol{p}} \delta\left(I(\boldsymbol{p}), l\right), \tag{1}$$

$$\delta(i, j) = \begin{cases} 1, & \text{if } i = j \\ 0, & \text{otherwise,} \end{cases} \tag{2}$$

where $l \in \{0, 1, 2, \cdots, l_{\mathrm{MAX}}\}$. The gradient norm of I at position $\boldsymbol{p}$ is denoted as $d(\boldsymbol{p})$. $d(\boldsymbol{p})$ is defined as follows [29]:

$$d(\boldsymbol{p}) = \sqrt{(d_{\mathrm{V}}(\boldsymbol{p}))^2 + (d_{\mathrm{H}}(\boldsymbol{p}))^2}, \tag{3}$$

$$d_{\mathrm{V}}(\boldsymbol{p}) = \begin{cases} d_{\mathrm{V,F}}(\boldsymbol{p}), & \text{if } |d_{\mathrm{V,F}}(\boldsymbol{p})| > |d_{\mathrm{V,B}}(\boldsymbol{p})| \\ d_{\mathrm{V,B}}(\boldsymbol{p}), & \text{otherwise,} \end{cases} \tag{4}$$

$$d_{\mathrm{V,F}}(\boldsymbol{p}) = \begin{cases} I(u, v) - I(u+1, v), & \text{if } u < U \\ 0, & \text{otherwise,} \end{cases} \tag{5}$$

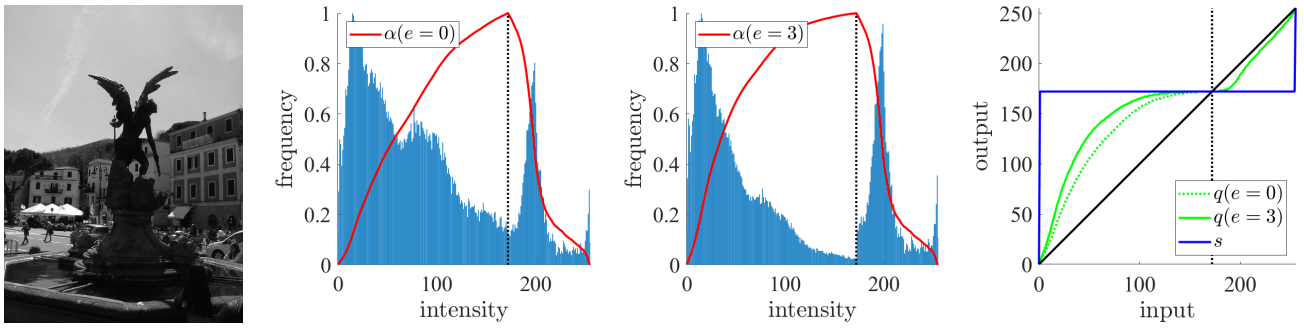

FIGURE 1. Examples of the weighted histogram, alpha value and tone curve. (a) Input image, (b) weighted histogram and alpha value ($e = 0$), (c) weighted histogram and alpha value ($e = 3$) and (d) tone curve ($e = 0, 3$). In (b) and (c), each value of the histogram is divided by the maximum frequency so that the maximum frequency is 1 (i.e., $\frac{h_w}{\max_l h_w(l)}$ is displayed). The dotted lines in (b) and (c) show the value of a.

$$d_{\mathrm{V,B}}(\boldsymbol{p}) = \begin{cases} 0, & \text{if } u = 1 \\ I(u,v) - I(u-1,v), & \text{otherwise,} \end{cases} \tag{6}$$

$$d_{\mathrm{H}}(\boldsymbol{p}) = \begin{cases} d_{\mathrm{H,F}}(\boldsymbol{p}), & \text{if } |d_{\mathrm{H,F}}(\boldsymbol{p})| > |d_{\mathrm{H,B}}(\boldsymbol{p})| \\ d_{\mathrm{H,B}}(\boldsymbol{p}), & \text{otherwise,} \end{cases} \tag{7}$$

$$d_{\mathrm{H,F}}(\boldsymbol{p}) = \begin{cases} I(u,v) - I(u,v+1), & \text{if } v < V \\ 0, & \text{otherwise,} \end{cases} \tag{8}$$

$$d_{\mathrm{H,B}}(\boldsymbol{p}) = \begin{cases} 0, & \text{if } v = 1 \\ I(u,v) - I(u,v-1), & \text{otherwise.} \end{cases} \tag{9}$$

B. GENERATION OF TONE CURVE

In this section, the method of generating the tone curve is described.

Let I be the input monochrome image. The proposed method first calculates the histogram h for I. Then Otsu binarization method [30] is applied to the portion of h that satisfies $l \geq l_{\mathrm{MID}}$. In the above process, the threshold t for dividing the histogram is calculated as follows:

$$t = \underset{l_{\mathrm{MID}} \leq l \leq l_{\mathrm{MAX}}}{\arg\max}\ g_{\mathrm{R1}}(l) g_{\mathrm{R2}}(l) (m_{\mathrm{R1}}(l) - m_{\mathrm{R2}}(l))^2, \tag{10}$$

$$g_{\mathrm{R1}}(l) = \sum_{l_{\mathrm{MID}} \leq d \leq l} h(d), \tag{11}$$

$$g_{\mathrm{R2}}(l) = \sum_{l < d \leq l_{\mathrm{MAX}}} h(d), \tag{12}$$

$$m_{\mathrm{R1}}(l) = \sum_{l_{\mathrm{MID}} \leq d \leq l} h(d) d, \tag{13}$$

$$m_{\mathrm{R2}}(l) = \sum_{l < d \leq l_{\mathrm{MAX}}} h(d) d. \tag{14}$$

After calculating t, a is calculated as follows:

$$a = \begin{cases} l_{\mathrm{MAX}}, & \text{if } \dfrac{\sum_{t < l \leq l_{\mathrm{MAX}}} h(l)}{UV} < 0.05 \\ t, & \text{otherwise} \end{cases}. \tag{15}$$

The weighted histogram h_w is calculated as follows:

$$h_w(l) = w_{\mathrm{E}}(l) \sum_{\boldsymbol{p}} d(\boldsymbol{p}) \delta\left(I(\boldsymbol{p}), l\right), \tag{16}$$

$$w_{\mathrm{E}}(l) = \begin{cases} \exp\left(-e \dfrac{l}{l_{\mathrm{MAX}}}\right), & \text{if } l \leq a \\ 1, & \text{otherwise.} \end{cases} \tag{17}$$

In Eq. (17), e is a parameter and its effect will be explained later. After calculating h_w, the tone curve $q(l)$ is generated as follows:

$$q(l) = \mathrm{round}\left(\alpha(l) s(l) + (1 - \alpha(l))\, l\right), \tag{18}$$

$$s(l) = \begin{cases} 0, & \text{if } l = 0 \\ a, & \text{else if } 0 < l < l_{\mathrm{MAX}} \\ l_{\mathrm{MAX}}, & \text{otherwise,} \end{cases} \tag{19}$$

$$\alpha(l) = \begin{cases} \dfrac{\sum_{0 \leq d \leq l} h_w(d)}{\sum_{0 \leq d \leq a} h_w(d)}, & \text{if } l \leq a \\ 1 - \dfrac{\sum_{a < d \leq l} h_w(d)}{\sum_{a < d \leq l_{\mathrm{MAX}}} h_w(d)}, & \text{otherwise.} \end{cases} \tag{20}$$

Figure 1 shows examples of the weighted histogram, alpha value and tone curve generated by the proposed method. Figure 1(a) shows the input image. Figure 1(b) shows the weighted histogram and alpha value calculated for the image shown in Fig. 1(a) when $e = 0$. Figure 1(c) shows the weighted histogram and alpha value calculated for the image shown in Fig. 1(a) when $e = 3$. Figure 1(d) shows the tone curve calculated for the image shown in Fig. 1(a) when $e = 0$ and $e = 3$. In Figs. 1(b) and 1(c), each value of the histogram is divided by the maximum frequency so that the maximum frequency is 1 (i.e., $\frac{h_w}{\max_l h_w(l)}$ is displayed). The dotted line in Figs. 1(b) and 1(c) show the value of a. As shown in Figs. 1(b) and 1(c), by increasing the value of e, the weighted histogram becomes more biased toward darker regions and the value of α becomes larger. In Fig. 1(d), it can be seen that the tone curve generated by the proposed method darkens very bright regions while brightening dark regions. It also can be seen that the effect of brightening dark regions becomes greater by increasing e. In Fig. 1, the slope of q increases with the slope of α. Since the slope of α at l increases with $h_w(l)$, the tone curve has a contrast enhancement effect. On the other hand, h_w is constructed

taking into account the gradient norm, which suppresses over-enhancement in the flat regions [29].

(a) (b)

FIGURE 2. Effect of local contrast correction. (a) and (b) are Q and O calculated for the image shown in Fig. 1(a), respectively.

C. LOCAL CONTRAST CORRECTION

As shown in Fig. 1(d), the slope of the tone curve becomes small when l takes the value close to a. This indicates that the tone curve may decrease the local contrast in the detailed regions whose local average pixel value is close to a. To suppress contrast reduction in such regions, the proposed method performs local contrast correction after applying the tone curve. In the local contrast correction, first a bilateral filter [26], [27], [28] is applied to I. The filtering output is denoted as $\bar{I}$. Let Q and O be the resultant image of the intensity conversion by q and the output of the local contrast correction, respectively. The pixel value of O is calculated as follows:

$$O(\boldsymbol{p}) = \text{round}\left(\alpha(\bar{I}(\boldsymbol{p}))I(\boldsymbol{p}) + \left(1 - \alpha(\bar{I}(\boldsymbol{p}))\right) Q(\boldsymbol{p})\right). \quad (21)$$

In Eq. (21), $O(\boldsymbol{p})$ becomes close to $Q(\boldsymbol{p})$ when the local average pixel value around $\boldsymbol{p}$ is not close to a. On the other hand, $O(\boldsymbol{p})$ becomes close to $I(\boldsymbol{p})$ when the local average pixel value around $\boldsymbol{p}$ is close to a. By controlling the effect of q in such a region-adaptive manner, the contrast reduction caused by the tone curve is suppressed. Figures 2(a) and 2(b) show Q and O obtained for the image shown in Fig. 1(a), respectively. The stone pattern is not visible at the edge of the fountain in the lower left area of the image in Q (Fig. 2(a)), whereas it is clearly visible in O (Fig. 2(b)).

Figure 3 shows an overview of the proposed method for monochrome images. Each process of the proposed method, such as gradient calculation, histogram calculation and bilateral filtering, is simple and suitable for fast implementation.

D. COLOR IMAGE PROCESSING

In this section, the proposed method to be applied to a color image is described.

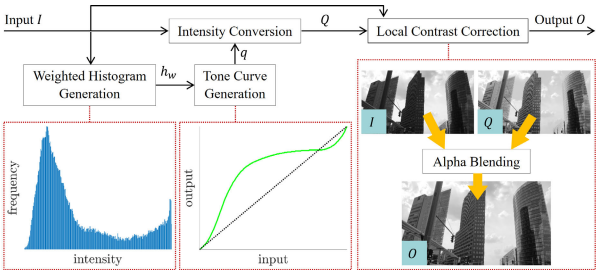

FIGURE 3. Overview of the proposed method for monochrome images.

Let $\boldsymbol{I}$ be the input color image. In the proposed method, monochrome image I is first obtained using the following equation:

$$I(\boldsymbol{p}) = \text{round}\left(\frac{R(\boldsymbol{p}) + G(\boldsymbol{p}) + B(\boldsymbol{p})}{3}\right), \quad (22)$$

where $R(\boldsymbol{p})$, $G(\boldsymbol{p})$ and $B(\boldsymbol{p})$ are the R, G and B components of $\boldsymbol{I}$ at position $\boldsymbol{p}$, respectively. Then, O is obtained by applying the algorithm described in sects. III-B and III-C. Let $\boldsymbol{O}$ be the output color image. The pixel value of $\boldsymbol{O}$ at position $\boldsymbol{p}$ is calculated as follows:

$$\boldsymbol{O}(\boldsymbol{p}) = \text{round}\left(\min\left(\frac{O(\boldsymbol{p})}{\max\left(I(\boldsymbol{p}), \varepsilon\right)}\boldsymbol{I}(\boldsymbol{p}), l_{\text{MAX}}\right)\right), \quad (23)$$

where ε is a small constant for avoiding division by 0. $\boldsymbol{I}(\boldsymbol{p})$ and $\boldsymbol{O}(\boldsymbol{p})$ are the RGB color vectors of I and $\boldsymbol{O}$ at position $\boldsymbol{p}$, respectively.

IV. EXPERIMENT

A. EXPERIMENTAL SETTINGS

To verify the effectiveness of the proposed method, a comparative experiment was conducted for the 254 images shown in Fig. 4. HE, CLAHE [8], Wang et al.'s method [18], SRIE [15], ZERO-DCE [25], Ueda et al.'s method [23], Akai et al.'s method [24], Hao et al.'s method [17], Buades et al.'s method [21] and Mukaida et al.'s method [10] were used as comparative methods. In the proposed method, the parameter e was set to be 3 and the spatial and range sigmas of a bilateral filter were set to $\lceil 0.03 \min(U, V) \rceil$ and 0.2, respectively. These parameters were set as the subjectively best parameters. Note that the bilateral filtering was applied after normalizing the pixel values to be in the range [0, 1].

B. QUANTITATIVE EVALUATION METRICS

As a quantitative evaluation, we used lightness order error (LOE) [31], [32], [33], NIQE [34], BIQME [35] and CR. The LOE was proposed to quantitatively evaluate the naturalness preservation performance. In this experiment, LOE [31], [32], [33] is calculated as follows:

$$\text{LOE} = \frac{\sum_{\boldsymbol{p}} \sum_{\boldsymbol{q}} F(L(\boldsymbol{p}), L(\boldsymbol{q})) \oplus F(L'(\boldsymbol{p}), L'(\boldsymbol{q}))}{U^2 V^2}, \quad (24)$$

$$F(x, y) = \begin{cases} 1, & \text{if } x \geq y \\ 0, & \text{otherwise,} \end{cases} \quad (25)$$

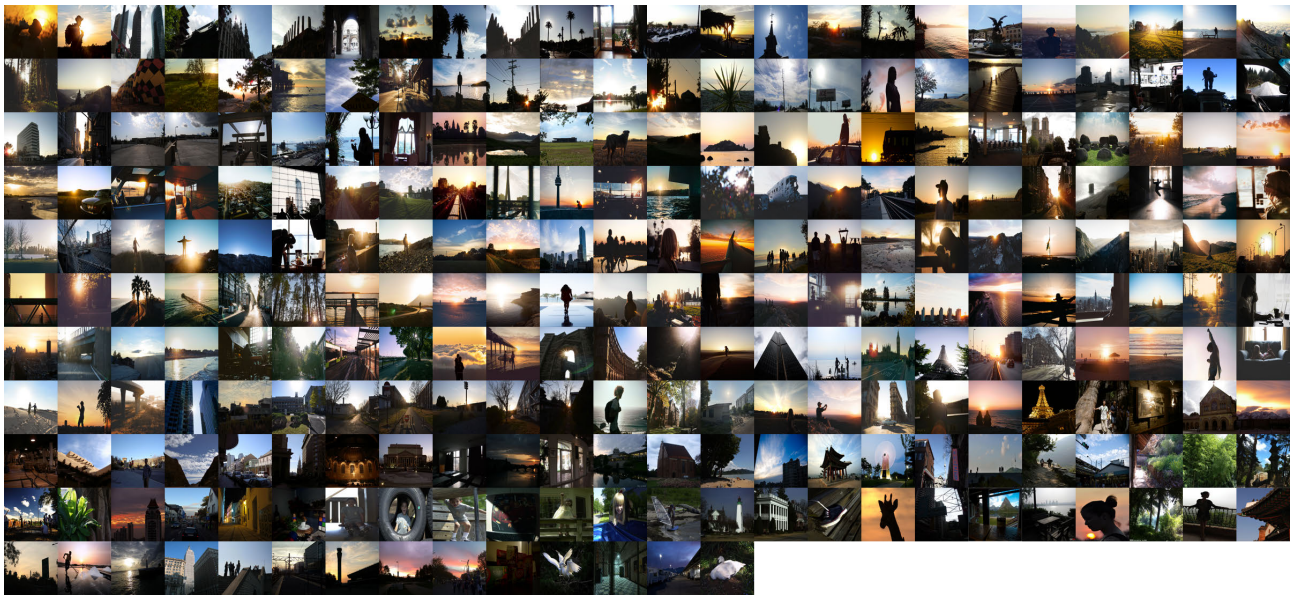

FIGURE 4. Test images.

where $L(\boldsymbol{p})$ and $L(\boldsymbol{q})$ are the maximum RGB values in the input image at positions $\boldsymbol{p}$ and $\boldsymbol{q}$, respectively. $L'(\boldsymbol{p})$ and $L'(\boldsymbol{q})$ are the maximum RGB values in the output image at positions $\boldsymbol{p}$ and $\boldsymbol{q}$, respectively. In accordance with [33], the calculations of Eqs. (24) and (25) were conducted after resizing the images by the factor of $\frac{50}{\min(U,V)}$. The lower the LOE value, the better the result. The NIQE [34] was proposed to quantitatively evaluate the image quality in terms of noise and blur. The low NIQE value indicates that the negative effects of noise and blur are small in the resulting image. BIQME [35] is a learning-based image quality metric taking into account the contrast, brightness and naturalness. The larger BIQME value indicates a higher image quality. CR is defined as follows:

$$\mathrm{CR} = \frac{100}{UV} \sum_{\boldsymbol{p}} (1 - H(I(\boldsymbol{p}))) \, H(O(\boldsymbol{p})), \tag{26}$$

$$H(l) = \begin{cases} 1, & \text{if } l = 0 \\ 1, & \text{else if } l = l_{\mathrm{MAX}} \\ 0, & \text{otherwise.} \end{cases} \tag{27}$$

In Eq. (26), I and O are the monochrome images converted from the input and output images, respectively. The color image to monochrome image conversion was performed in the same way as in Eq. (22). The low CR value indicates that black-out and white-out were suppressed.

C. EXPERIMENTAL RESULTS

Figures 5–9 show examples of the experimental results for various wide-dynamic-range scenes. In Figs. 5–9, (a) show the input images and (b)–(l) show the results of HE, CLAHE, Wang et al.'s method, SRIE, ZERO-DCE, Ueda et al.'s method, Akai et al.'s method, Hao et al.'s method, Buades et al.'s method, Mukaida et al.'s method and the proposed method, respectively. In Figs. 5–7, (m)–(x) are the enlarged excerpts of boxed regions of (a)–(l).

As can be seen from Figs. 5(f), 5(g) and 5(k), ZERO-DCE, Ueda et al.'s method and Mukaida et al.'s method generated low-contrast images. On the other hand, we see from Fig. 5(l) that the proposed method was able to generate a high-contrast and high-visibility image. Figures 5(o) and 5(p) show that CLAHE and Wang et al.'s method caused over-enhancement, which resulted in amplifying small noise. Figure 5(q) shows that SRIE caused a halo artifact around a round electric light. As can be seen from Fig. 5(x), the proposed method was able to suppress the halo artifact and noise amplification.

As can be seen from Figs. 6(f), 6(g), 6(j) and 6(k), ZERO-DCE, Ueda et al.'s method, Buades et al.'s method and Mukaida et al.'s method generated low-contrast images. Figures 6(o) and 6(u) show that CLAHE and Hao et al.'s method caused white-out. Figures 6(l) and 6(x) show that the proposed method was able to generate a natural and high-visibility image.

Figure 7(b) shows that HE caused severe over-enhancement and generated a low-visibility image. Figure 7(c) shows that CLAHE was not able to brighten the dark regions and generated a low-visibility image. Figure 7(i) shows that Hao et al.'s method decreased the local contrast in some regions and flattened the image details. As can be seen from Figure 7(t), the visibility of the paving stones is low in the result of Akai et al.'s method. Figures 7(l) and 7(x) show that the proposed method was able to brighten the dark regions and enhance the visibility of image details.

As can be seen from Figs. 8(b), 8(c), 8(d), 8(e) and 8(i), HE, CLAHE, Wang et al.'s method, SRIE and Hao et al.'s

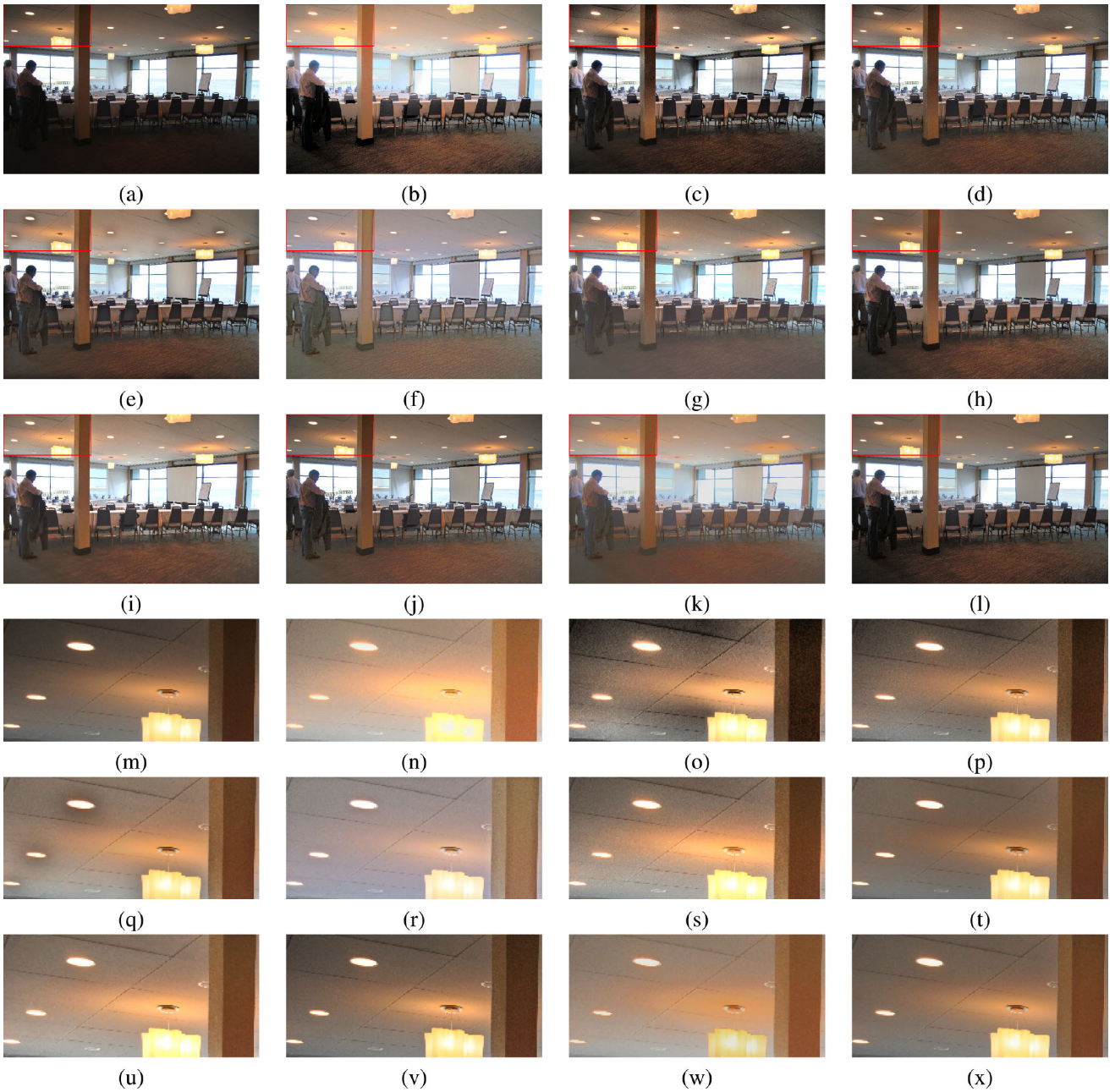

FIGURE 5. Experimental results for image 1. (a) is the input image. (b)–(l) are the results of HE, CLAHE, Wang et al.'s method, SRIE, ZERO-DCE, Ueda et al.'s method, Akai et al.'s method, Hao et al.'s method, Buades et al.'s method, Mukaida et al.'s method and the proposed method, respectively. (m)–(x) are the enlarged excerpts of boxed regions of (a)–(l).

method were not able to brighten the dark foreground region sufficiently. Figure 8(f) shows that ZERO-DCE improved the visibility by brightening the dark foreground region, but caused contrast reduction and an undesired color change in the background, resulting in an unnatural image. Figure 8(g) shows that Ueda et al.'s method caused black-out in the dark foreground region. Figure 8(l) shows that the proposed method generated a sufficiently bright image preserving the image naturalness.

Figure 9(b) shows that HE decreased the contrast in bright regions around the street lights. As can be seen from Figs. 9(f), 9(j) and 9(k), ZERO-DCE, Buades et al.'s method and Mukaida et al.'s method generated low-contrast images. As can be seen from Figs. 9(d), 9(e), 9(f) and 9(k), Wang et al.'s method, SRIE, ZERO-DCE and Mukaida et al.'s method caused roughness in the dark sky region. As can be seen from Figure 9(h), Akai et al.'s method generated an unnatural and low-visibility image. Figure 9(l) shows that

FIGURE 6. Experimental results for image 2. (a) is the input image. (b)–(l) are the results of HE, CLAHE, Wang et al.'s method, SRIE, ZERO-DCE, Ueda et al.'s method, Akai et al.'s method, Hao et al.'s method, Buades et al.'s method, Mukaida et al.'s method and the proposed method, respectively. (m)–(x) are the enlarged excerpts of boxed regions of (a)–(l).

the proposed method generated a natural and high-visibility image.

Figure 10 shows the results of the quantitative evaluation in terms of LOE, NIQE and BIQME. In each box plot, the box represents the range from the first quartile q_1 to the third quartile q_3. The whiskers represent the maximum and minimum scores in the range $[q_1 - 1.5(q_3 - q_1), q_3 + 1.5(q_3 - q_1)]$. The horizontal line in the box represents the median and the cross represents the mean. In Fig. 10, "Prop." means the proposed method. Figure 10(a) shows that CLAHE and Buades et al.'s method tended to generate worse scores for LOE than the other methods. On the other hand, the proposed method generated better scores for LOE than the most other methods. This indicates that the proposed method did not disrupt the lightness order structure of the image considerably and tended to produce a natural output image. Figure 10(b) shows that Wang et al.'s method and CLAHE tended to generate worse scores for NIQE than the other methods. This indicates that these methods tended to cause over-enhancement and amplify

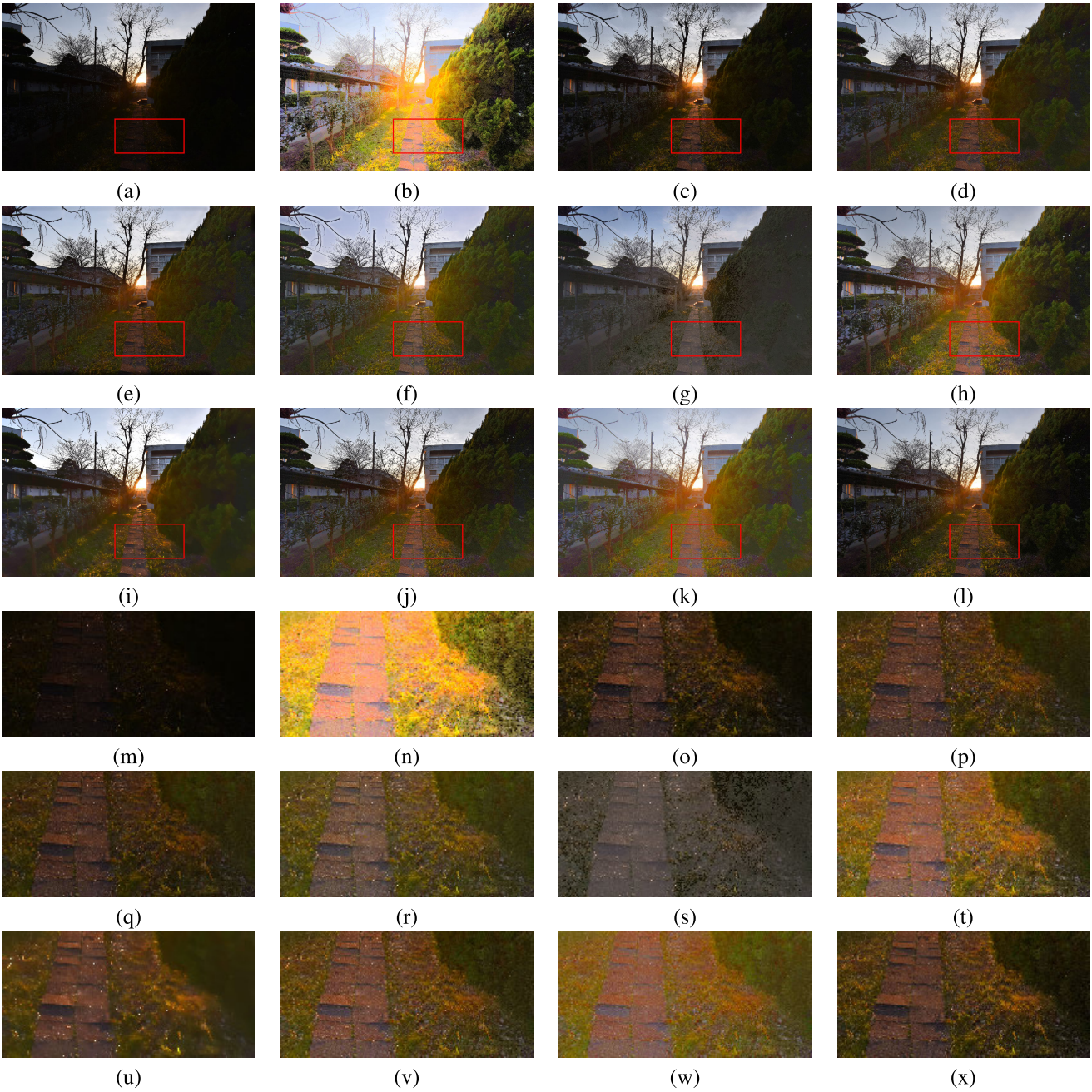

FIGURE 7. Experimental results for image 3. (a) is the input image. (b)–(l) are the results of HE, CLAHE, Wang et al.'s method, SRIE, ZERO-DCE, Ueda et al.'s method, Akai et al.'s method, Hao et al.'s method, Buades et al.'s method, Mukaida et al.'s method and the proposed method, respectively. (m)–(x) are the enlarged excerpts of boxed regions of (a)–(l).

small noise. As can be seen from Fig. 10(b), the proposed method tended to generate better scores for NIQE than Wang et al.'s method and CLAHE. This indicates that the proposed method was able to suppress over-enhancement compared with Wang et al.'s method and CLAHE. Figure 10(c) shows that ZERO-DCE, Ueda et al.'s method and Mukaida et al.'s method have more variations in BIQME values and lower average values than the other methods. This indicates that ZERO-DCE, Ueda et al.'s method and Mukaida et al.'s method were often unable to adjust brightness and enhance contrast sufficiently. Figure 10(c) shows that the proposed method stably generated favorable scores for BIQME. This indicates that the proposed method stably produced sufficient visibility enhancement effects. The averages of CR for the test images are summarized in Table1. Table1 shows that HE, Ueda et al.'s method, Hao et al.'s method and

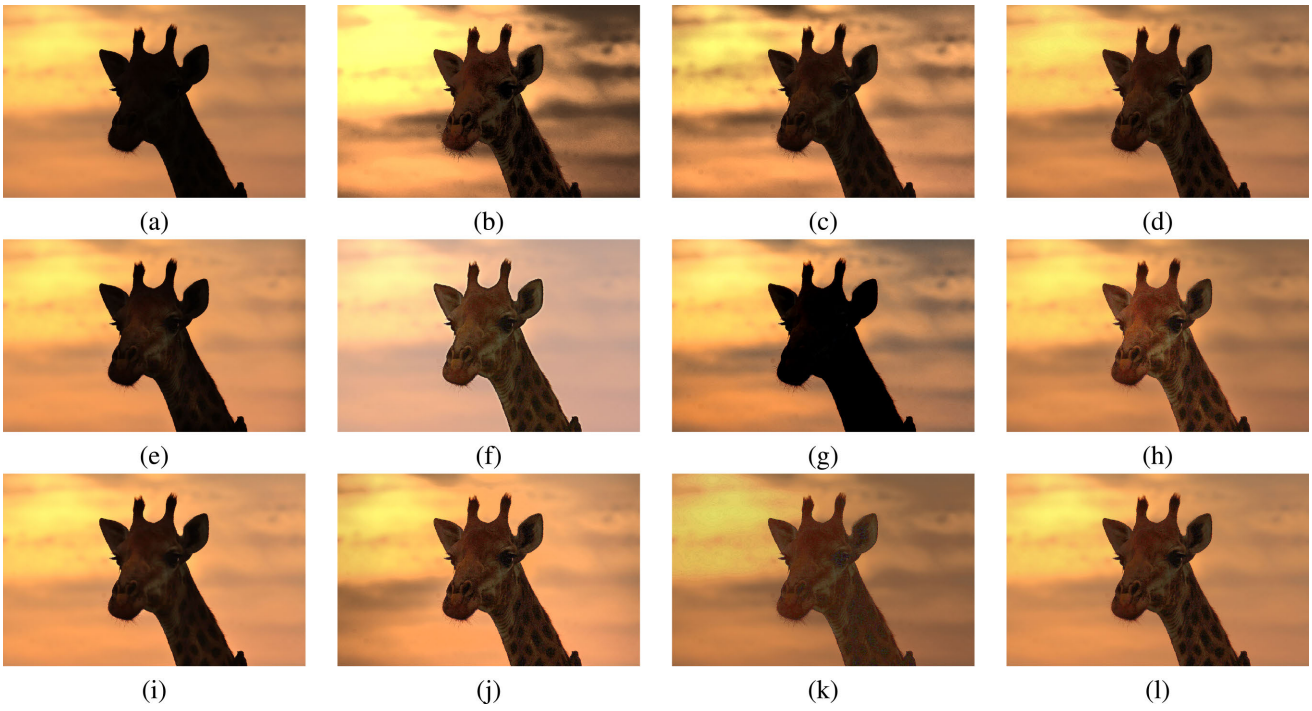

FIGURE 8. Experimental results for image 4. (a) is the input image. (b)–(l) are the results of HE, CLAHE, Wang et al.'s method, SRIE, ZERO-DCE, Ueda et al.'s method, Akai et al.'s method, Hao et al.'s method, Buades et al.'s method, Mukaida et al.'s method and the proposed method, respectively.

FIGURE 9. Experimental results for image 5. (a) is the input image. (b)–(l) are the results of HE, CLAHE, Wang et al.'s method, SRIE, ZERO-DCE, Ueda et al.'s method, Akai et al.'s method, Hao et al.'s method, Buades et al.'s method, Mukaida et al.'s method and the proposed method, respectively.

Buades et al.'s method generated higher CR values than the other methods. This indicates that HE, Ueda et al.'s method, Hao et al.'s method and Buades et al.'s method often caused white-out or black-out. On the other hand,

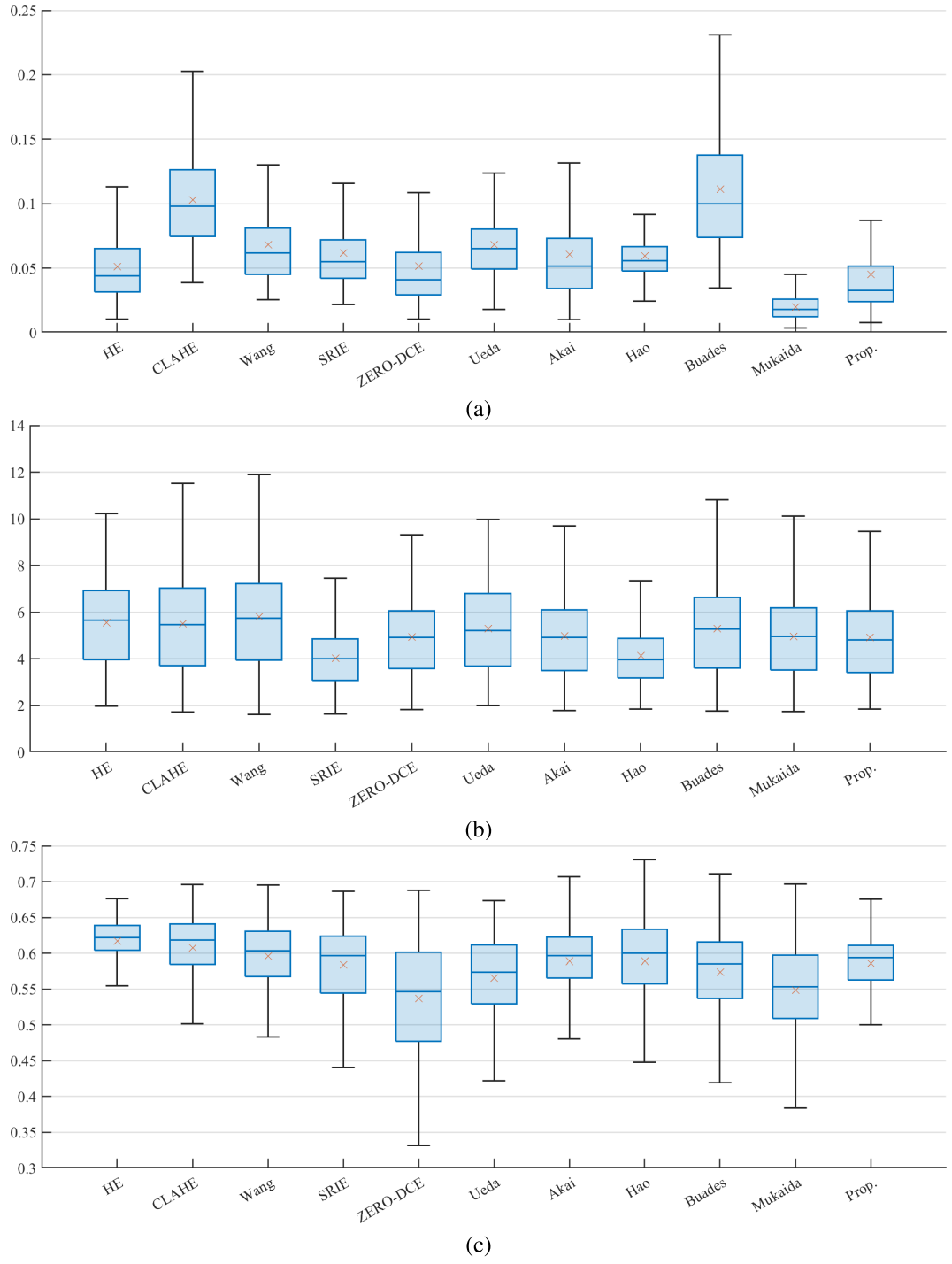

FIGURE 10. Quantitative evaluation results. (a) LOE, (b) NIQE and (c) BIQME.

Table1 shows that the proposed method suppressed such over-enhancement.

The processing times taken by HE, CLAHE, Wang et al.'s method, SRIE, Ueda et al.'s method, Akai et al.'s method, Hao et al.'s method, Mukaida et al.'s method and the proposed method for the image shown in Fig. 8(a), which has 573 pixels in height and 900 pixels in width, are summarized in Table 2. The execution environment is as follows: CPU: AMD-Ryzen7-5700G-3.80 GHz, Memory: 16 GB, OS: Window 11 and Language: MATLAB R2023a. For Buades et al.'s method, there is no measurement result as we used the online code. In [25], it is reported that ZERO-DCE can process a 640 × 480 pixel image in about 0.002 seconds when using a GPU. It can be considered that the balance between the

performance of image enhancement and the processing speed of the proposed method was confirmed.

TABLE 1. Average CR values for all test images.

Method	CR
HE	0.502
CLAHE	0.002
Wang et al.'s method	0.072
SRIE	0.034
ZERO-DCE	0.027
Ueda et al.'s method	0.232
Akai et al.'s method	**0**
Hao et al.'s method	0.920
Buades et al.'s method	0.331
Mukaida et al.'s method	0.001
Prop.	**0**

TABLE 2. The processing times taken by HE, CLAHE, Wang et al.'s method, SRIE, Ueda et al.'s method, Akai et al.'s method, Hao et al.'s method, Mukaida et al.'s method and the proposed method for the image shown in Fig. 8(a).

Method	Processing time (in second)
HE	**0.01**
CLAHE	0.02
Wang et al.'s method	0.24
SRIE	9.61
Ueda et al.'s method	10.13
Akai et al.'s method	0.10
Hao et al.'s method	3.22
Mukaida et al.'s method	0.14
Prop.	0.09

V. CONCLUSION

In this paper, we proposed an image enhancement method for the images captured in wide-dynamic-range scenes. In the proposed method, a tone curve for improving visibility was generated by using the gradient-norm-based weighted histogram. The tone curve generated by the proposed method was able to achieve both brightness adjustment and contrast enhancement preserving image naturalness. After applying the tone curve to the input image, the proposed method performed the local contrast correction for suppressing local contrast reduction in the detailed region. In the local contrast correction, the input image and the resultant image of the tone curve were merged by alpha blending.

The experiment using various evaluation metrics confirmed the effectiveness of the proposed method in terms of visibility enhancement performance and naturalness preservation performance. In addition, the proposed method was also confirmed to perform well in terms of processing speed.

Note that the proposed method is very simple and easy to implement. Hence, the proposed method can be easily used as a pre-processing step for applications used in embedded devices, which require low power consumption and memory usage. As a future task, we are considering the development of a dedicated algorithm specialized for videos.

REFERENCES

[1] T. Mertens, J. Kautz, and F. Van Reeth, "Exposure fusion: A simple and practical alternative to high dynamic range photography," *Comput. Graph. Forum*, vol. 28, no. 1, pp. 161–171, Mar. 2009.
[2] Z. G. Li, J. H. Zheng, and S. Rahardja, "Detail-enhanced exposure fusion," *IEEE Trans. Image Process.*, vol. 21, no. 11, pp. 4672–4676, Nov. 2012.
[3] M. Nejati, M. Karimi, S. M. R. Soroushmehr, N. Karimi, S. Samavi, and K. Najarian, "Fast exposure fusion using exposedness function," in *Proc. IEEE Int. Conf. Image Process. (ICIP)*, Sep. 2017, pp. 2234–2238.
[4] K. Ma, H. Li, H. Yong, Z. Wang, D. Meng, and L. Zhang, "Robust multi-exposure image fusion: A structural patch decomposition approach," *IEEE Trans. Image Process.*, vol. 26, no. 5, pp. 2519–2532, May 2017.
[5] Q. Wang, W. Chen, X. Wu, and Z. Li, "Detail-enhanced multi-scale exposure fusion in YUV color space," *IEEE Trans. Circuits Syst. Video Technol.*, vol. 30, no. 8, pp. 2418–2429, Aug. 2020.
[6] H. Li, K. Ma, H. Yong, and L. Zhang, "Fast multi-scale structural patch decomposition for multi-exposure image fusion," *IEEE Trans. Image Process.*, vol. 29, pp. 5805–5816, 2020.
[7] R. C. Gonzalez and R. E. Woods, *Digital Image Processing* (Histogram Processing), 4th ed. London, U.K.: Pearson, 2018, ch. 3.3.
[8] K. Zuiderveld, "Contrast limited adaptive histogram equalization," *Graph. Gems*, vol. 4, pp. 474–485, Jan. 1994.
[9] S.-C. Huang, F.-C. Cheng, and Y.-S. Chiu, "Efficient contrast enhancement using adaptive gamma correction with weighting distribution," *IEEE Trans. Image Process.*, vol. 22, no. 3, pp. 1032–1041, Mar. 2013.
[10] M. Mukaida, Y. Ueda, and N. Suetake, "Low-light image enhancement method using a modified gamma transform and gamma filtering-based histogram specification for convex combination coefficients," *IEICE Trans. Fundam. Electron., Commun. Comput. Sci.*, vol. E106.A, no. 11, pp. 1385–1394, Nov. 2023.
[11] Y. Ueda and N. Suetake, "Hue-preserving color image enhancement on a vector space of convex combination coefficients," in *Proc. IEEE Int. Conf. Image Process. (ICIP)*, Sep. 2019, pp. 939–943.
[12] M. Mukaida, Y. Ueda, and N. Suetake, "Low-light image enhancement method by using a modified gamma transform for convex combination coefficients," in *Proc. IEEE Int. Conf. Image Process. (ICIP)*, Oct. 2022, pp. 2866–2870.
[13] D. J. Jobson, Z. Rahman, and G. A. Woodell, "Properties and performance of a center/surround retinex," *IEEE Trans. Image Process.*, vol. 6, no. 3, pp. 451–462, Mar. 1997.
[14] D. J. Jobson, Z. Rahman, and G. A. Woodell, "A multiscale retinex for bridging the gap between color images and the human observation of scenes," *IEEE Trans. Image Process.*, vol. 6, no. 7, pp. 965–976, Jul. 1997.
[15] X. Fu, D. Zeng, Y. Huang, X.-P. Zhang, and X. Ding, "A weighted variational model for simultaneous reflectance and illumination estimation," in *Proc. IEEE Conf. Comput. Vis. Pattern Recognit. (CVPR)*, Jun. 2016, pp. 2782–2790.
[16] X. Guo, Y. Li, and H. Ling, "LIME: Low-light image enhancement via illumination map estimation," *IEEE Trans. Image Process.*, vol. 26, no. 2, pp. 982–993, Feb. 2017.
[17] S. Hao, X. Han, Y. Guo, X. Xu, and M. Wang, "Low-light image enhancement with semi-decoupled decomposition," *IEEE Trans. Multimedia*, vol. 22, no. 12, pp. 3025–3038, Dec. 2020.
[18] Q. Wang, X. Fu, X.-P. Zhang, and X. Ding, "A fusion-based method for single backlit image enhancement," in *Proc. IEEE Int. Conf. Image Process. (ICIP)*, Sep. 2016, pp. 4077–4081.
[19] G. Deng, "A generalized unsharp masking algorithm," *IEEE Trans. Image Process.*, vol. 20, no. 5, pp. 1249–1261, May 2011.
[20] N. Kojima, B. Lamsal, N. Matsumoto, and M. Yamashiro, "Proposing autotuning image enhancement method using stochastic resonance," *Electron. Commun. Jpn.*, vol. 102, no. 4, pp. 35–46, Apr. 2019.

[21] A. Buades, J. Lisani, A. B. Petro, and C. Sbert, "Backlit images enhancement using global tone mappings and image fusion," *IET Image Process.*, vol. 14, no. 2, pp. 211–219, Feb. 2020.
[22] Y. Ueda, D. Moriyama, T. Koga, and N. Suetake, "Histogram specification-based image enhancement for backlit image," in *Proc. IEEE Int. Conf. Image Process. (ICIP)*, Oct. 2020, pp. 958–962.
[23] Y. Ueda, T. Koga, and N. Suetake, "Fusion-based backlit image enhancement using multiple S-type transformations for convex combination coefficients," in *Proc. IEEE Int. Conf. Image Process. (ICIP)*, Oct. 2022, pp. 2971–2975.
[24] M. Akai, Y. Ueda, T. Koga, and N. Suetake, "Low-artifact and fast backlit image enhancement method based on suppression of lightness order error," *IEEE Access*, vol. 11, pp. 121231–121245, 2023.
[25] C. Guo, C. Li, J. Guo, C. C. Loy, J. Hou, S. Kwong, and R. Cong, "Zero-reference deep curve estimation for low-light image enhancement," in *Proc. IEEE/CVF Conf. Comput. Vis. Pattern Recognit. (CVPR)*, Jun. 2020, pp. 1777–1786.
[26] C. Tomasi and R. Manduchi, "Bilateral filtering for gray and color images," in *Proc. 6th Int. Conf. Comput. Vis.*, Jan. 1998, pp. 839–846.
[27] S. Paris and F. Durand, "A fast approximation of the bilateral filter using a signal processing approach," in *Proc. 9th Eur. Conf. Comp. Vis.*, 2006, pp. 568–580.
[28] J. Chen, S. Paris, and F. Durand, "Real-time edge-aware image processing with the bilateral grid," *ACM Trans. Graph.*, vol. 26, no. 3, p. 103, Jul. 2007.
[29] Y. Ueda, T. Koga, H. Misawa, N. Suetake, and E. Uchino, "Gradient-norm-based histogram equalization taking account of HSV color space distribution," *Opt. Rev.*, vol. 24, no. 3, pp. 406–415, Jun. 2017.
[30] N. Otsu, "A threshold selection method from gray-level histograms," *IEEE Trans. Syst. Man, Cybern.*, vol. SMC-9, no. 1, pp. 62–66, Jan. 1979.
[31] S. Wang, J. Zheng, H.-M. Hu, and B. Li, "Naturalness preserved enhancement algorithm for non-uniform illumination images," *IEEE Trans. Image Process.*, vol. 22, no. 9, pp. 3538–3548, Sep. 2013.
[32] L. Li, R. Wang, W. Wang, and W. Gao, "A low-light image enhancement method for both denoising and contrast enlarging," in *Proc. IEEE Int. Conf. Image Process. (ICIP)*, Sep. 2015, pp. 3730–3734.
[33] Z. Ying, G. Li, Y. Ren, R. Wang, and W. Wang, "A new low-light image enhancement algorithm using camera response model," in *Proc. IEEE Int. Conf. Comput. Vis. Workshops (ICCVW)*, Oct. 2017, pp. 3015–3022.
[34] A. Mittal, R. Soundararajan, and A. C. Bovik, "Making a 'completely blind' image quality analyzer," *IEEE Signal Process. Lett.*, vol. 20, no. 3, pp. 209–212, Mar. 2013.
[35] K. Gu, D. Tao, J.-F. Qiao, and W. Lin, "Learning a no-reference quality assessment model of enhanced images with big data," *IEEE Trans. Neural Netw. Learn. Syst.*, vol. 29, no. 4, pp. 1301–1313, Apr. 2018.

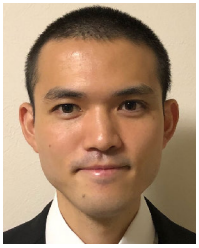

SEIICHI KOJIMA (Graduate Student Member, IEEE) received the B.Sc. degree from Kyoto University, Japan, in 2016, and the M.S. degree from Yamaguchi University, Japan, in 2020, where he is currently pursuing the Ph.D. degree in science. His research interests include low-light image enhancement and high-dynamic-range imaging. He is a Student Member of IEICE.

NORIAKI SUETAKE (Member, IEEE) received the B.E., M.E., and Ph.D. degrees in control engineering and science from the Kyushu Institute of Technology, Japan, in 1992, 1994, and 2000, respectively. He is currently a Professor with the Graduate School of Sciences and Technology for Innovation, Yamaguchi University, Japan. His research interests include digital signal processing, image processing, and intelligent systems. He is a member of Optica and IEICE.